Study of the Anisotropic Reflectance Behaviour of Wheat Canopy to Evaluate the Performance of Radiative Transfer Model PROSAIL5B

Debasish Chakraborty · Vinay Kumar Sehgal ·
Rabi Narayan Sahoo · Sanatan Pradhan ·
Vinod Kumar Gupta

Abstract A field experiment was conducted on wheat to analyze its bi-directional reflectance in relation to sun-target-sensor geometry. To achieve a large variation in crop parameters, two extreme nitrogen treatments were applied. The study reconfirms the strong and consistent anisotropic patterns of wheat bi-directional reflectance in visible (VIS) and near infra-red (NIR) and its magnitude was highest in the principal plane. This anisotropic pattern extended equally in shortwave infra-red (SWIR). The hotspot broadened with crop growth due to increase in leaf area index (LAI), leaf size and planophilic orientation. The shape and magnitude of PROSAIL5B simulated spectra was in close agreement with the observed spectra in the optical region for most of the view zenith and azimuth angle combinations. In the NIR and SWIR, the magnitude of the model simulations showed good match in the principal plane, whereas underestimation was found in the backward scattering direction at higher view zenith angles in the VIS. The typical bowl shape of observed reflectance in principal plane was very well simulated in NIR by the model but failed in other wavebands. The model performed best in the NIR region followed by SWIR and maximum relative error was in VIS. Over the whole optical region and view zenith angles, the model simulations showed an average error of 26%. The model simulations were poor at low LAI indicating the need to improve soil reflectance algorithm in the model. Results of the study have implications for understanding the strengths/shortcomings in the model and its inversion to derive crop biophysical parameters from multispectral sensors.

Keywords Bi-directional reflectance · Crop · Hotspot · Modeling · Inversion

D. Chakraborty · V. K. Sehgal (✉) · R. N. Sahoo · S. Pradhan ·
V. K. Gupta
Division of Agricultural Physics, Indian Agricultural Research
Institute (IARI), New Delhi 110012, India
e-mail: vksehgal@gmail.com

V. K. Sehgal
e-mail: sehgal@iari.res.in

D. Chakraborty
e-mail: debasishagri@gmail.com

R. N. Sahoo
e-mail: rnsahoo.iari@gmail.com

S. Pradhan
e-mail: sanatan28@gmail.com

V. K. Gupta
e-mail: vk_001@gmail.com

Introduction

Estimation of vegetation biochemical and biophysical variables with reasonable accuracy has usefulness for a range of agricultural, ecological, and meteorological applications (Houborg et al. 2007; Darvishzadeh et al. 2008). Leaf area index (LAI), leaf chlorophyll content (LCC) and leaf water content (C_w) are the most important vegetation parameters among all (Houborg et al. 2007). The two common approaches for estimating vegetation parameters from remotely sensed data are: (a) Empirical/statistical and (b) Physical. But the statistical relationships being sensor-specific and dependent on site and sampling conditions, are supposed to change in space and time (Meroni et al. 2004). The physical approach involving radiative transfer models (RTM) can accurately describes the spectral variation of canopy reflectance as a function of canopy, leaf and soil background characteristics (Goel 1989; Meroni et al. 2004) by explaining the transfer and interaction of radiation inside the canopy based on physical laws (Houborg et al. 2007).

The earth and plant surface features reflect radiation aniso-tropically. So the observed reflectance of a remotely sensed scene (with respect to a Lambertian reference) alters with the source and view geometry and is quantified as "bi-directional reflectance factor" (BRF). The BRF is not only a function of relative geometry of illumination and observation, but also depends on the biochemical composition of vegetation surface (leaf pigments, intercellular space, moisture content) and the spatial and geometrical arrangement of surface elements (shape, size and orientation of leaves, mutual shading). So, the inversion of bi-directional canopy reflectance models emerged as a promising alternative for retrieval of vegetation biophysical parameters (Goel 1989). The new generation of space borne instruments likes POLDER (Polarization and Directionality of the Earth′s reflectance) and MISR (Multi-angle Imaging Spectroradiometer) on board ADEOS (Advance Earth Observing Satellite) and Terra, respectively, are designed to study both the spectral and directional reflectance of the earth surface.

Research on use of radiative transfer models (RTMs) for crop biophysical parameter retrieval has emerged as an area of scientific pursuit globally in last one decade (Meroni et al. 2004; Houborg et al. 2007; Yao et al. 2008; Vohland and Jarmer 2008). The RTM inversion requires thorough validation of the model for target crops at various growth stages under different growing condi-tions, followed by analysis of model′s shortcomings. Though many studies have analyzed the bi-directional reflectance behaviour of vegetation canopies using spectroradiometers mounted on a variety of goniometers (Roman et al. 2011), only a few have pursued detailed evulation of the model simulations of bi-directional re-flectance at various growth stages under different growing conditions (Andrieu et al. 1997; Sridhar et al. 2009; Barman et al. 2010). Most of the studies have not been exhaustive to measure BRF in the whole optical domain from 400–2,500 nm, at different growth stages of crop and for crop experiencing extreme treatments resulting in varied crop growth. There is a merit in undertaking de-tailed field evaluation of canopy reflectance models under such varying crop growth conditions to evaluate their strengths and shortcomings for the purpose of their in-formed applications.

Keeping this background in view, the bi-directional reflec-tance of wheat was studied at different source-target-view geometries, at two growth stages and under contrasting grow-ing conditions in the optical region (400–2,500 nm). Further, the bi-directional reflectance measurements were used to eval-uate the performance of model PROSAIL5B. This study specifically validated model at two growth stages of wheat which were grown under two contrasting treatments of nitro-gen application, thus resulting in a large variation in crop biophysical parameters.

Methodology

Study Area

The field experiment was conducted in the experimental farm of the Indian Agricultural Research Institute, New Delhi which is located at 28°38'23" N latitude and 77°09'27" E longitude with an altitude of 228.6 m above mean sea level. The soil here is sandy loam in texture, deep and with moderate fertility. The site is having semi-arid climate with two distinct crop seasons, viz., *kharif* (Jun-Oct) and *rabi* (Nov-Mar).

Experimental Detail

Spring wheat (*Triticum aestivum* L.) variety PBW-502 was grown during the *rabi* season of 2010–2011 with two nitrogen treatments, each with three replications in a plot size of 6 m× 6 m. The treatments were applied with the objective to create variability in crop growth vis-à-vis vegetation biophysical and biochemical parameters. Crop was sown on November 25, 2010 by seed drill at a recommended row spacing of 22.5 cm. Two nitrogen treatments, namely, 0 (N_0) and 120 (N_{120}) kg ha^{-1} were applied. The full nitrogen dose was applied in three splits - half as basal and one fourth each as topdressing at crown-root-initiation (CRI) stage and flowering stage. The recommended dose of phosphorous and potassium was ap-plied as basal. Lowest chlorophyll and poor growth was realized in N_0 treatment resulting in sparse canopy. Highest chlorophyll with better growth was realized in N_{120} treatment resulting in a well developed dense canopy.

Measurements of Plant Parameters

Various plant parameters, to be used as input for PROSAIL model, were measured on same day synchronizing with the spectral observations taken at different growth stages. Five plants were randomly selected in each plot and their height was measured with a metric scale. Leaf length of second mature leaf from the top of these five plants in each plot was also measured by a metric scale and averaged. Leaf Area Index (LAI) was measured using Plant Canopy Analyser (LI-2000) following the procedure given by Welles and Norman (1991). Multiple LAI observations (at least five) on each date within each plot were taken and their average was calculated to represent LAI of that plot on that date. Leaf angle in degrees was measured using a protractor. All leaves on one plant and five such plants in each plot were sampled for leaf angle measurement and their average leaf angle (A*ngl*) with respect to horizontal was calculated. For leaf chlorophyll content (C_{ab}) measurements, 50 mg of fresh leaf samples from different treatments were weighed accurately on an analytical balance and chlorophyll was extracted by a non macerated method, equilibrating it with 10 ml DiMethyl SulfOxide

(DMSO) in a capped vial and keeping in an oven at 65 °C for about 3 h (Hiscox and Israelstam 1979). The decanted solution was used to estimate the absorbance at 645 and 663 nm wavelengths using Spectrophotometer. Plant samples were cut just above the soil surface and their leaves were separated. The area of fresh leaves was determined by passing them through leaf-area meter (LI-3100). These leaves were dried in an oven at 70 °C to achieve a constant weight and then their dry weight was recorded. The specific leaf weight (C_m) was calculated as the ratio of dry weight of leaves to leaf area of the same sample. Equivalent leaf moisture thickness (C_w), an index of leaf water content which represents volume of leaf water per unit leaf area, was calculated as the ratio of difference in fresh and dry leaf weight to leaf area.

Bi-directional Reflectance Measurements

The BRF measurements were recorded between 11:00 and 13:00 h under clear sky conditions using hand-held Spectroradiometer (ASD FieldSpec-3) installed on a portable field goniometer (same setup was used as described in Barman et al. 2010). The spectroradiometer is having a default 25° Field of View (FOV) which was decreased to 10° using fore-optics provided with the instrument. The reflectance were measured at 1 nm interval in the spectral range of 350–2,500 nm at eight relative azimuthal angles (i.e. relative to the azimuth angle of sun) of 0°, 45°, 90°, 135°, 180°, 225°/-135°, 270°/-90° and 315°/-45°, and at six zenith angles of 20°, 30°, 40°, 50° and 60° plus nadir. In principal plane (which is aligned to sun azimuth), 0° relative azimuth refers to the backward scattering direction of light while 180° relative azimuth refers to the forward scattering direction of light. Corresponding to each view azimuth and zenith position, reflectance was also recorded from a reference panel coated with barium sulphate, reflecting about 99 % radiation. Time taken for making these measurements was about 20–25 min during which we assumed a fixed position of sun at that location.

Bi-directional Reflectance Analysis

In order to analyze the BRF pattern of crop, BRF surface plots were prepared at four wavelengths corresponding to the central wavelengths of IRS-P6 LISS-3 (Indian Remote Sensing Satellite-P6, Linear Imaging Self Scanning-3) bands, viz., 568, 660, 790 and 1,634 nm. The 41 spectral reflectance values corresponding to all the view zenith and relative azimuth angles were interpolated using "smoothing spline" function to generate a surface of bi-directional reflectance. The surface plots were prepared in rectangular coordinate system where view-zenith angle was plotted on x-axis (varying diagonally), relative-azimuth angle on y-axis (varying horizontally) and spectral reflectance on z-axis. Before plotting, the spherical

coordinates of view zenith and relative azimuth angles were transformed into rectangular coordinates. The bi-directional surface plots at four wavelengths were prepared for N_0 and N_{120} treatments and compared.

The Radiative Transfer Model PROSAIL

This study used a variant of one of the widely applied canopy radiative transfer model PROSAIL (Jacquemoud et al. 2009) which is a combination of two models, i.e., the PROSPECT model (Jacquemoud and Baret 1990) that describes leaf optical properties and the SAIL model (Verhoef 1984) that computes canopy reflectance at different wavelengths. The PROSAIL model considers the detailed information on leaf optical properties and also accounts for hotspot effect. The PROSAIL5B version of model (downloaded from http://teledetection.ipgp. jussieu.fr/prosail/) was used in this study which incorporates PROSPECT-5 and 4SAIL models. The input parameters of PROSAIL5B with their units are given in Table 1.

Validation of PROSAIL

In order to validate the model for a given treatment on a particular day, required input parameters of leaf, canopy, soil, view and solar zenith and relative azimuth angles were provided. The model then simulated canopy bi-directional reflectance between 400 and 2,500 nm at 1 nm interval. The performance of the model was evaluated by comparing model simulated values with observed values in two ways: (a) for the whole spectra and (b) at specific wavelengths. In case of whole spectra validation, the observed spectra in the range of 400–2,500 nm at different view zenith angles in the principal plane were compared with the corresponding model

Table 1 Input parameters of PROSAIL5B model

Parameters	Description
Ihot	Hot spot flag (1=use hot spot)
Angl	Average leaf angle (°)
LAI	Leaf Area Index (m^2 m^{-2})
N	Structural Coefficient (unit less)
Cab	Chlorophyll a + b content (μg cm^{-2})
Car	Carotenoid content (μg cm^{-2})
Cbrown	Brown pigment content (arbitrary units)
Cw	Leaf Equivalent Water Thickness (cm)
Cm	Leaf Dry matter Content (g cm^{-2})
Hspot	Hot-spot parameter (Leaf length/Crop height)
Skyl	Percent Diffuse to Direct radiation
Psoil	Soil Coefficient
Theta_S	Solar Zenith Angle (°)
Theta_O	Observer zenith angle (°)
Psi	Relative Azimuth Angle (°)

simulated spectra. It helped in evaluating the performance of the model to simulate the variation in the reflectance due to the variation in the view zenith angles. The portions of spectra between 1,350–1,400 nm, 1,800–2,000 nm and 2,400–2,500 nm were not considered for comparison due to the presence of significant atmospheric noise in the observed spectra. Again for the validation of the model at specific wavelengths, simulated values were validated by comparing them with observed values at specific wavelengths (568, 660, 790 and 1,634 nm) which corresponded to the central wavelength of IRS-P6 LISS-3 spectral bands. In this case also the validation was done in the principal plane at different view zenith angles (−60°, −50°, −40°, −30°, −20°, 0°, 20°, 30°, 40°, 50°, 60°). The negative view zenith referred to backward scattering direction (i.e. sun behind sensor) and the positive referred to forward scattering direction (i.e. sensor opposite to sun).

Model Performance Evaluation

The performance of the model was evaluated by calculating Root Mean Square Error (RMSE) between observed and model simulated reflectance values, either at particular wavelength or for a wavelength band using formula given below:

$$RMSE = \sqrt{\frac{\sum_{i=1}^{n}(R_{obs} - R_{sim})^2}{n}} \qquad (1)$$

where, R_{obs} is observed reflectance, R_{sim} is simulated reflectance, and n is number of observations.

In order to compare RMSE across wavelength regions and at various growth stages of the crop, it was normalized by the average of observed reflectance values and thus normalized RMSE (nRMSE) was calculated as given below:

$$nRMSE = \frac{RMSE}{\mu} \qquad (2)$$

where, μ is mean of observed reflectance values.

For whole spectra comparison, the RMSE and nRMSE were calculated for wavelength regions 400–700 nm (VIS), 800–1,300 nm (NIR) and 1,500–2,400 nm (SWIR) and are referred to as *RMSE1, RMSE2, RMSE3* and *nRMSE1, nRMSE2* and *nRMSE3*, respectively.

Results

Measured Parameters

The measured values of PROSAIL parameters for wheat with their standard deviation for two nitrogen treatments (N_0 and N_{120}) on 46 and 106 days after sowing (DAS) are given in Table 2. The *LAI* was 0.48 and 0.60 on 46 DAS which increased to 1.7 and 3.2 on 106 DAS in N_0 and N_{120} treatments, respectively. The effect of nitrogen treatment on *LAI* was little during initial growth stages (46 DAS) which became more pronounced at later growth stages (106 DAS). In case of C_{ab}, the effect of nitrogen treatment was evident at all the growth stages of wheat as chlorophyll content is very sensitive to the nitrogen availability. The variations in the C_w were limited as crop was not exposed to any water treatment during its growth season. Similarly, the range of variations in C_m was less across treatments and DAS. The leaves were more erect on 46 DAS as shown by *Angl* value of 70° but became less erect on 106 DAS with *Angl* value ranging between 35 and 45°. On 46 DAS, the *Hspot* value was 0.78–0.79 under both the treatments and the value decreased to 0.22 in N_0 and 0.32 in N_{120} at 106 DAS. These varied observations constituted a good dataset for analyzing the anisotropic behaviour of wheat canopy reflectance and validation of PROSAIL5B over a range of crop biophysical conditions.
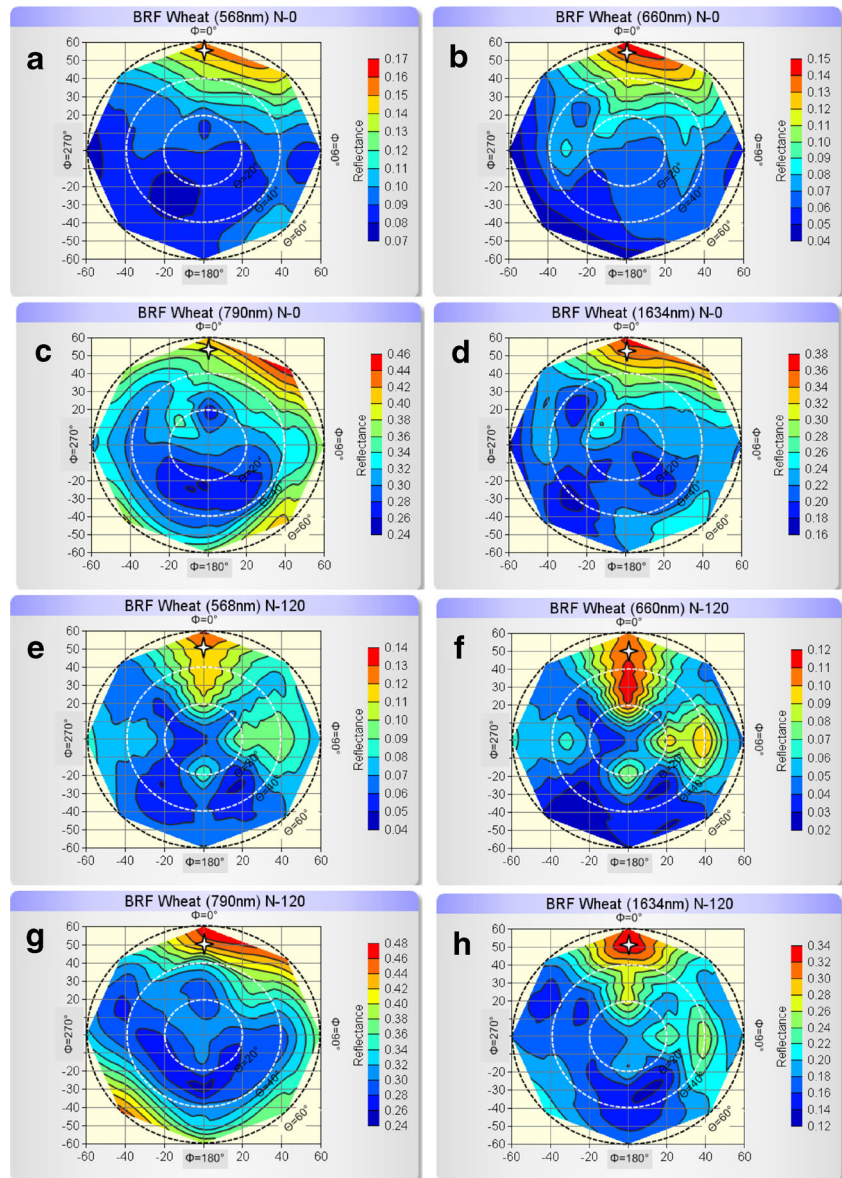
Bi-directional Reflectance Patterns

Figure 1 and 2 shows the bi-directional reflectance patterns at 46 DAS and 106 DAS for N_0 and N_{120} treatments,

Table 2 Field measured values of wheat parameters with their standard deviation (SD) for N_0 and N_{120} nitrogen treatments at 46 and 106 DAS

Parameters	Description	N_0				N_{120}			
		46 DAS		106 DAS		46 DAS		106 DAS	
		Mean	SD	Mean	SD	Mean	SD	Mean	SD
LAI	Leaf Area Index (m² m⁻²)	0.48	0.02	1.70	0.07	0.60	0.18	3.20	0.22
Cab	Chlorophyll a+b content (µg cm⁻²)	28	1.92	29	4.14	52	6.62	65	8.82
Cw	Leaf Equivalent Water Thickness (cm)	0.033	0.003	0.027	0.0016	0.024	0.0012	0.030	0.0022
Cm	Leaf Dry matter Content (g cm⁻²)	0.0071	0.0004	0.0031	0.0006	0.0046	0.0002	0.0047	0.0003
Angl	Average leaf angle (°)	70	2.41	35	2.56	70	2.06	45	1.60
Hspot	Hot-spot parameter (Leaf length/Crop height)	0.79	0.055	0.22	0.014	0.78	0.034	0.32	0.013

Fig. 1 Polar plots showing bi-directional reflectance factor (BRF) of wheat for N_0 at (**a**) 568 nm, (**b**) 660 nm, (**c**) 790 nm and (**d**) 1,634 nm and for N_{120} at (**e**) 568 nm, (**f**) 660 nm, (**g**) 790 nm and (**h**) 1,634 nm, 46 DAS


respectively. The symbol of star in these figures depicts the position of sun at the time of observations. The bi-directional reflectance was analyzed at four wavelengths corresponding to central wavelengths of IRS-P6 LISS-3 bands. These selected wavelengths also represent different mechanisms of interaction of radiation with plant canopy.

Figure 1 show the bi-directional reflectance pattern of wheat on 46 DAS when solar zenith angle was 51°. It shows wide variations in reflectance at a given wavelength with change in sun-target-sensor geometry. Overall, in both the treatments and at all the wavelengths, higher reflectance was observed in backward scattering direction than in forward. Highest reflectance was invariably observed in the principal plane between 50° and 60° view zenith angles and 0° relative azimuth which corresponded to the hot-spot position. An exception was at 790 nm for N_0 where hot-spot occurred at

45° relative azimuth instead of 0°. The hot-spot was very well marked in N_{120} treatment than in N_0. In both the treatments, the reflectance at 790 nm (NIR) was higher at view zenith angle of 50°–60° for all relative azimuth angles but such pattern was not observed at other wavelengths. The N_0 treatment showed a little higher reflectance than N_{120} at 568, 660 and 1,634 nm but the trend was reversed at 790 nm. It may be noted that the minimum reflectance at 568, 660 and 1,634 nm was found at 60^0 view zenith angle in forward scattering direction (relative azimuth 180°, 225° and 270°) but for 790 nm it was found at about 20° view zenith angle in forward scattering direction in both the treatments.

Figure 2 shows the bi-directional reflectance pattern of wheat on 106 DAS when solar zenith angle was 33°. The bi-directional reflectance pattern showed higher reflectance in backward scattering direction and lower

Fig. 2 Polar plots showing bi-directional reflectance factor (BRF) of wheat for N$_0$ at (**a**) 568 nm, (**b**) 660 nm, (**c**) 790 nm and (**d**) 1,634 nm and for N$_{120}$ at (**e**) 568 nm, (**f**) 660 nm, (**g**) 790 nm and (**h**) 1,634 nm, 106 DAS
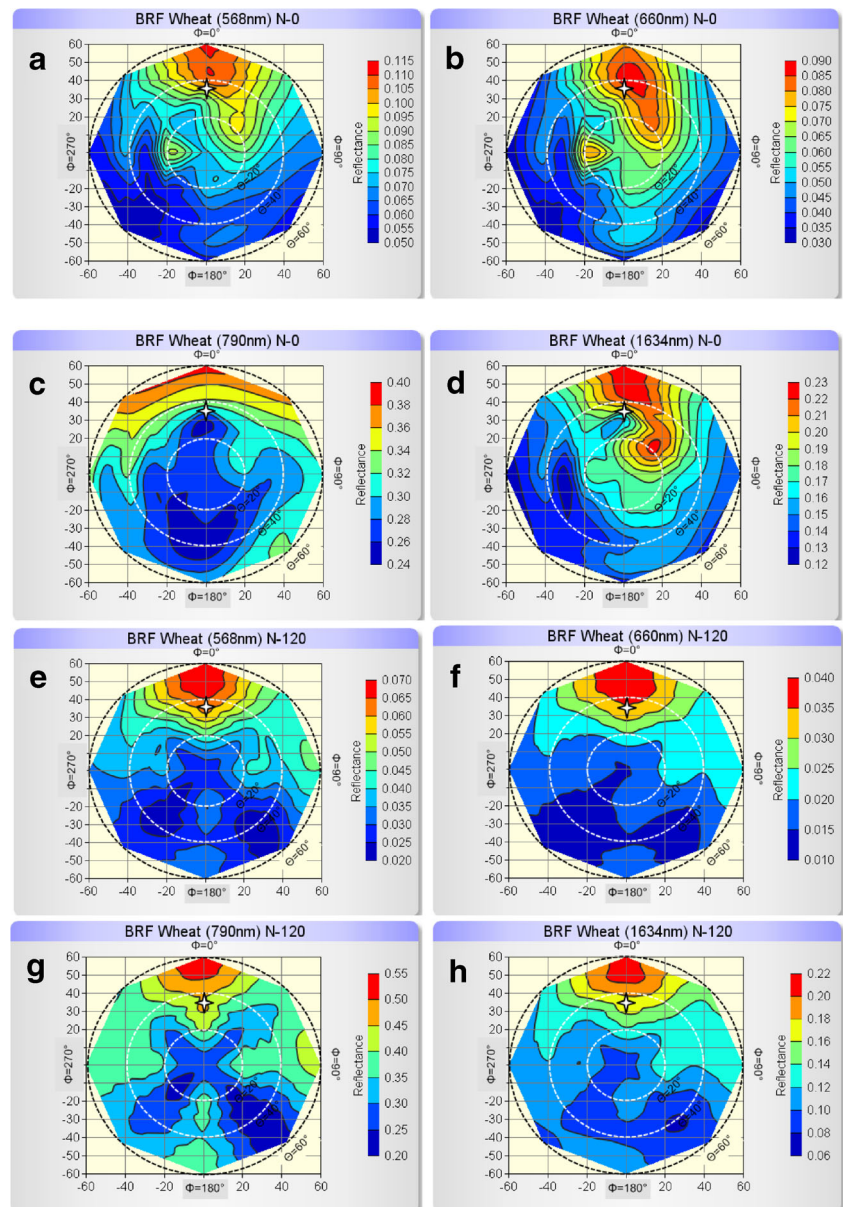
reflectance in forward scattering direction at all the four wavelengths in both the treatments. The pattern of bi-directional reflectance at 106 DAS showed broadening of the maximum reflectance zone, i.e. hotspot for all the selected wavelengths in both the treatments. The extent of broadening was lower at 790 nm in both the treatments than at other wavelengths. The minimum reflectance was found in the forward scattering direction rather than at the nadir view position. At 790 nm wavelength, reflectance increased with increase in view zenith angle at all relative azimuth angles in both the treatments. Again the maximum reflectance in both the treatments at 568 and 660 nm was found in the range of 35–50° view zenith angles in backward scattering direction and minima was in forward scattering direction just opposite to that.

These patterns match the typical vegetation BRF and reconfirm the anisotropic radiation scattering behaviour of wheat canopy. The bi-directional reflectance at all the wavelengths generally increased for off-nadir view angles. At all wavelengths, the bi-directional reflectance was higher in backscatter direction than forward scatter direction. The hotspot (maximum reflectance) occurred in principal plane in backward scattering direction and its position synchronized with the sun zenith angle. The reflectance at 790 nm (NIR) was generally more systematic around nadir than at the other three wavelengths.

Validation of PROSAIL Model

The model PROSAIL-5B was validated for wheat crop at specific wavelengths in the principal plane. Results are presented for N_0 and N_{120} treatments at 46 and 106 DAS which represented wide variation in leaf biochemical and canopy biophysical parameters. The default values of parameters $Car=1$ µg.cm^{-2} and $Cbrown=0.05$ were used. The leaf structural parameter N, whose value ranges between 1.0 to 1.5 for monocotyledonous plants (Jacquemoud 1993), was specified a value of $N=1.0$. The value $N=1.0$ was found to best fit the model simulated spectra with the observed spectra in most of the cases. The value of percent diffuse to direct sunlight (skyl) was assumed to be of 10 because all the spectroradiometeric observations were taken under clear sky conditions. The parameter $psoil=0.1$ was found to best fit the observed spectra of shaded soil in field with that of model generated soil spectra. The Figs. 3 and 4 show that the model performance varied across different view zenith angles in backward and forward scattering directions, respectively. The performance of the model (in terms of RMSE and nRMSE) in principal plane at

different wavebands across treatments at two dates are summarized in Table 3.

The model simulated well the canopy spectra maintaining a close resemblance in terms of shape with that of the observed spectra at different view zenith angles in the principal plane on 106 DAS (Figs. 3 and 4). The observed spectra showed increase in reflectance with increase in zenith angle and model also showed similar result indicating model's sensitivity to variation in view zenith angle. The RMSE1, RMSE2 and RMSE3 in backward scattering ranged between 0.01–0.02, 0.02–0.05 and 0.01–0.04, respectively. The RMSE1, RMSE2 and RMSE3 in forward scattering direction were nearly same with a value of 0.01. The model performed better in the forward scattering direction than in the backward scattering direction across the optical region. In backward scattering direction, the model errors were highest at higher zenith angles of 50–60°.

In absolute terms, the N_0 treatment showed better match in VIS and SWIR bands than in NIR band at all view zenith angles throughout the principal plane as indicated by lower magnitude of RMSE1 (0.02–0.03) and RMSE3 (0.01–0.09)

Fig. 3 Comparison of model simulated and observed spectral reflectance in principal plane for N_{120} treatment at different view zenith angles in the backward scattering direction on 106 DAS. (RAz is Relative Azimuth Angle; Vz is View/ Sensor Zenith Angle)
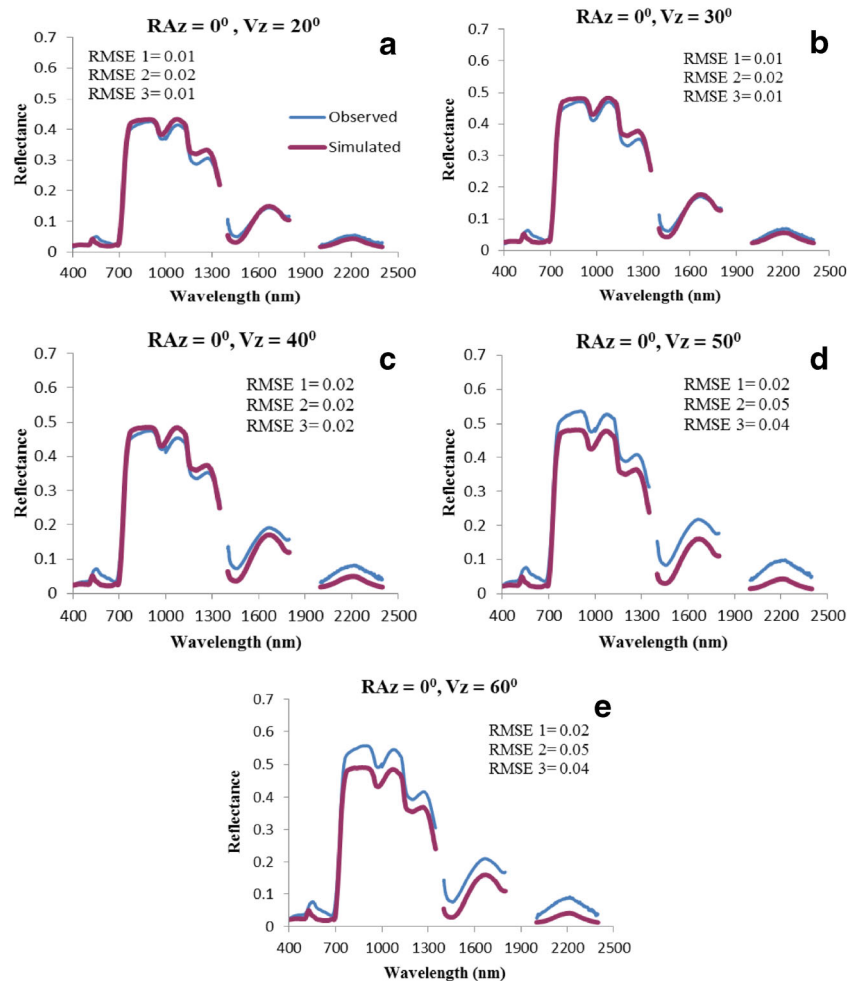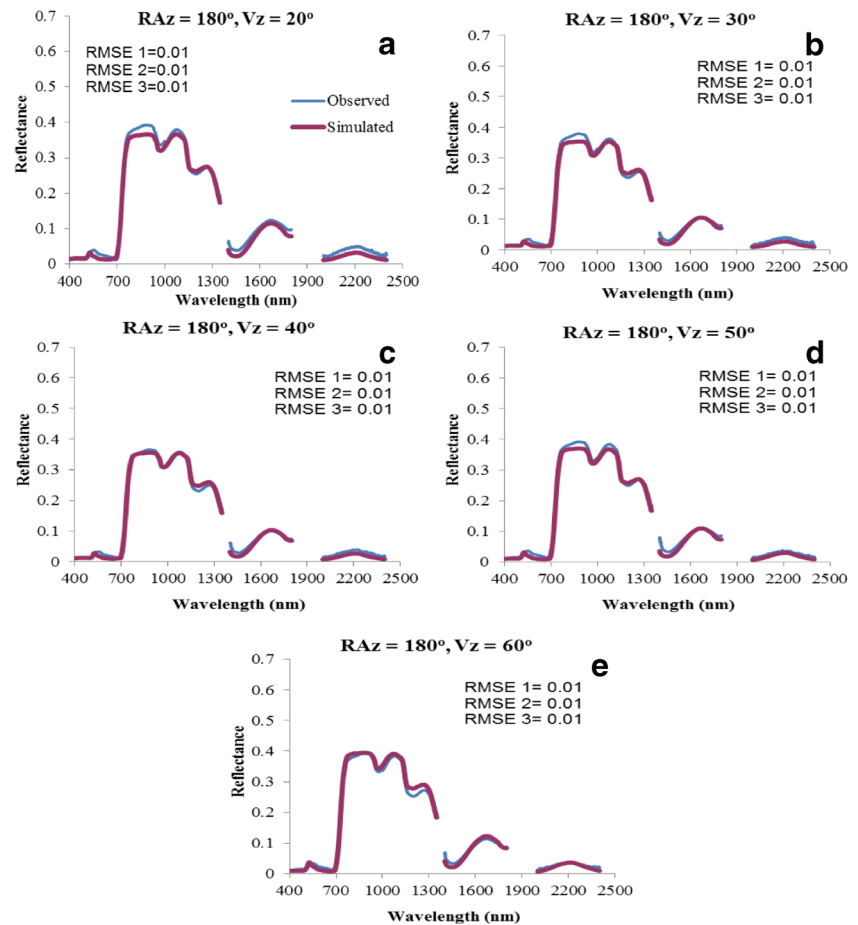
Fig. 4 Comparison of model simulated and observed spectral reflectance in the principal plane for N_{120} treatment at different view zenith angles in the forward scattering direction on 106 DAS. (RAz is Relative Azimuth Angle; Vz is View/ Sensor Zenith Angle)

than *RMSE2* (0.02–0.13) at 46 DAS (Table 3). For N_{120} treatment, same trend was observed. But the *nRMSE* indicates that the relative error (as percent of mean band reflectance) was highest in VIS band (mean *nRMSE1* = 0.38 and 0.33) in both the treatments (Table 3). Moreover, the simulated peak in VIS band was shifted to lower wavelength of 525 nm than the observed peak around 550 nm, in both backward and forward scattering directions. The NIR band simulation was better in N_{120} than in N_0 as indicated by lower mean nRMSE value of 0.14 as against a value of 0.21. Overall, *RMSE* and *nRMSE* variations were lower in N_{120} treatment than in N_0 treatment indicating poor performance of the model for sparser canopy.

In case of N_0 at 106 DAS, similar trend of higher nRMSE values in backward and lower in forward scattering were observed (Table 3). Exactly same trend was also observed for the N_{120} treatment with even better performance than in N_0, in both backward and forward scattering directions. In the case of N_{120}, the RMSEs in forward scattering direction were very low (about 0.01). But the mean *nRMSE* showed opposite trend and was highest for VIS in both the treatments. Similar to 46 DAS, the model performed much better for N_{120} than N_0. It again indicates that the model performs better for dense canopy than for sparse canopy.

The comparison of model simulated reflectance with observed values at four specific wavelengths (568, 660, 790, and 1,634 nm) in the solar principal plane (for −60° to +60° view zenith) for N_0 and N_{120} treatments on 46 DAS is shown in Fig. 5. In terms of reflectance magnitude, the performance of the model showed a reasonably good match in both the treatments. In both N_0 and N_{120} treatments, the model underestimated reflectance in the backward scattering, especially close to the hotspot. In forward scattering direction, model generally overestimated reflectance at all the wavelengths except at 790 nm wavelength where it underestimated reflectance throughout the principal plane. Observed reflectance showed a bowl shape with view zenith angle at all the wavelengths but this shape was very prominent at 790 nm indicating that off-nadir angles cause an increase in reflectance. The model simulated reflectance, though close to observed values, showed a very clear bowl shape only at 790 nm. Generally, a mismatch in the shapes was observed at 568, 660 and 1,634 nm wavelengths in all the cases.

The Fig. 6 shows that the model performed well in both the treatments as it could simulate the decrease in reflectance with increase in view zenith from −60° to +60° at all the four wavelengths on 106 DAS. In case of N_0, the model underestimated reflectance at 568, 660 and 1,634 nm while

Table 3 Root Mean Square Error (RMSE) and Normalized Root Mean Square Error (nRMSE) (values in parentheses) of N_0 and N_{120} treatments in different wavelength bands at 46 and 106 DAS in the solar principal plane

| DAS	Treatment	Wavelength Band	View Zenith Angle (Degree) in Solar Principal Plane											Mean RMSE (nRMSE)
			-60	-50	-40	-30	-20	0	+20	+30	+40	+50	+60	
46	N-0	400–700 nm	0.034 (0.30)	0.02 (0.21)	0.02 (0.20)	0.02 (0.22)	0.03 (0.37)	0.03 (0.46)	0.03 (0.52)	0.03 (0.49)	0.03 (0.48)	0.02 (0.44)	0.03 (0.55)	0.03 (0.39)
		800–1,300 nm	0.09 (0.19)	0.06 (0.15)	0.07 (0.19)	0.06 (0.17)	0.03 (0.10)	0.06 (0.21)	0.04 (0.15)	0.05 (0.18)	0.08 (0.26)	0.11 (0.35)	0.14 (0.38)	0.07 (0.21)
		1,500–2,400 nm	0.09 (0.30)	0.04 (0.15)	0.02 (0.09)	0.01 (0.05)	0.02 (0.13)	0.04 (0.26)	0.03 (0.16)	0.02 (0.13)	0.02 (0.12)	0.02 (0.13)	0.02 (0.18)	0.03 (0.15)
	N-120	400–700 nm	0.03 (0.36)	0.02 (0.24)	0.03 (0.33)	0.03 (0.34)	0.03 (0.34)	0.02 (0.61)	0.01 (0.12)	0.01 (0.23)	0.01 (0.35)	0.01 (0.31)	0.01 (0.36)	0.02 (0.33)
		800–1,300 nm	0.04 (0.08)	0.03 (0.07)	0.01 (0.02)	0.03 (0.09)	0.01 (0.05)	0.04 (0.15)	0.04 (0.16)	0.02 (0.08)	0.06 (0.21)	0.09 (0.31)	0.13 (0.36)	0.05 (0.14)
		1,500–2,400 nm	0.04 (0.18)	0.04 (0.18)	0.05 (0.21)	0.05 (0.23)	0.07 (0.28)	0.03 (0.28)	0.03 (0.20)	0.03 (0.28)	0.03 (0.31)	0.01 (0.19)	0.01 (0.09)	0.04 (0.28)
106	N-0	400–700 nm	0.04 (0.52)	0.04 (0.53)	0.04 (0.49)	0.03 (0.39)	0.03 (0.45)	0.02 (0.47)	0.03 (0.51)	0.02 (0.50)	0.02 (0.49)	0.02 (0.49)	0.01 (0.35)	0.03 (0.47)
		800–1,300 nm	0.01 (0.04)	0.01 (0.01)	0.02 (0.07)	0.09 (0.36)	0.04 (0.16)	0.01 (0.01)	0.01 (0.04)	0.01 (0.03)	0.01 (0.01)	0.01 (0.02)	0.01 (0.03)	0.02 (0.07)
		1,500–2,400 nm	0.07 (0.42)	0.07 (0.42)	0.06 (0.37)	0.03 (0.27)	0.05 (0.35)	0.05 (0.35)	0.05 (0.41)	0.05 (0.41)	0.04 (0.39)	0.04 (0.37)	0.02 (0.23)	0.05 (0.36)
	N-120	400–700 nm	0.02 (0.50)	0.02 (0.51)	0.02 (0.43)	0.01 (0.33)	0.01 (0.32)	0.01 (0.26)	0.01 (0.38)	0.01 (0.39)	0.01 (0.39)	0.01 (0.44)	0.01 (0.37)	0.01 (0.40)
		800–1,300 nm	0.05 (0.11)	0.05 (0.10)	0.02 (0.05)	0.02 (0.05)	0.02 (0.05)	0.09 (0.39)	0.01 (0.04)	0.01 (0.04)	0.01 (0.03)	0.01 (0.04)	0.01 (0.04)	0.03 (0.08)
		1,500–2,400 nm	0.04 (0.35)	0.04 (0.38)	0.02 (0.23)	0.01 (0.09)	0.01 (0.11)	0.01 (0.26)	0.01 (0.19)	0.01 (0.15)	0.01 (0.14)	0.01 (0.11)	0.01 (0.08)	0.01 (0.19)
		Mean RMSE (nRMSE)	0.05 (0.24)	0.04 (0.23)	0.03 (0.23)	0.03 (0.25)	0.03 (0.29)	0.03 (0.25)	0.02 (0.25)	0.02 (0.28)	0.03 (0.27)	0.03 (0.27)	0.03 (0.32)	0.03 (0.26)

it remained close at 790 nm. The *RMSE* values were 0.03, 0.04, 0.03 and 0.04 for 568, 660, 790 and 1,634 nm, respectively. The magnitude of underestimation was more in the backward scattering direction, particularly at 568 and 660 nm bands. A close match was observed at 790 and 1,634 nm in comparison to 568 and 660 nm. Model simulations were much better in N_{120} than in N_0 at all the four wavelengths as indicated by lower *RMSE* values of 0.024, 0.009, 0.042 and 0.025, respectively. The model performance significantly improved at 568 and 660 nm in N_{120} over N_0. Little but consistent underestimation was observed at 568 and 660 nm, especially in the backward scattering direction. Here also observed reflectance showed prominent bowl shape at 790. The model could also simulate bowl shape of reflectance at this wavelength. These results also indicate that the model performance is much better for dense canopy than for sparse.

Discussion

Bi-directional Reflectance Patterns

In this study, the bi-directional reflectance observed at different wavelengths and at different growth stages of wheat confirmed the typical highly anisotropic scattering behaviour of wheat canopy throughout the optical wavelength region as has been reported by Sridhar et al. (2009) and Barman et al. (2010). Anisotropic scattering of vegetation canopies generally results in increasing reflectance with off-nadir view angles (Donovan et al. 1985) and our results also showed similar pattern. As reported in literature (Kimes et al. 1984, Donovan et al. 1985 and Roman et al. 2011), our results also showed that the bi-directional reflectance was significantly higher in backward scattering direction than in forward scattering direction in the optical region. The Figs. 1 and 2 clearly showed that peak reflectance was observed in principal plane in backward scattering direction in the direction of the sun referred to as "hotspot". This pattern occurred for all the four wavelength bands centred at 568 (GREEN), 660 (RED), 790 (NIR) and 1,634 nm (SWIR) with the magnitude of reflectance being higher in the NIR, followed by SWIR and lowest in RED. Similar patterns have been reported by Kimes (1984) and Sridhar et al. (2009) in RED and NIR bands. Increasing reflectance with off-nadir viewing is a function of viewing different proportions of the canopy layers as the view zenith angle changes. As the view zenith angle increases, a higher percentage of upper canopy layers are viewed. The proportion of shadowed canopy to sunlit canopy layers increases with canopy depth. Thus, viewing a higher percentage of upper canopy layers than at nadir

Fig. 5 Comparison of the observed (square & line) and model simulated (triangle & dashed line) reflectance in the principal plane on 46 DAS for N_0 (blue) and N_{120} (red) at (**a**) 568 nm, (**b**) 660 nm, (**c**) 790 nm and (**d**) 1,634 nm
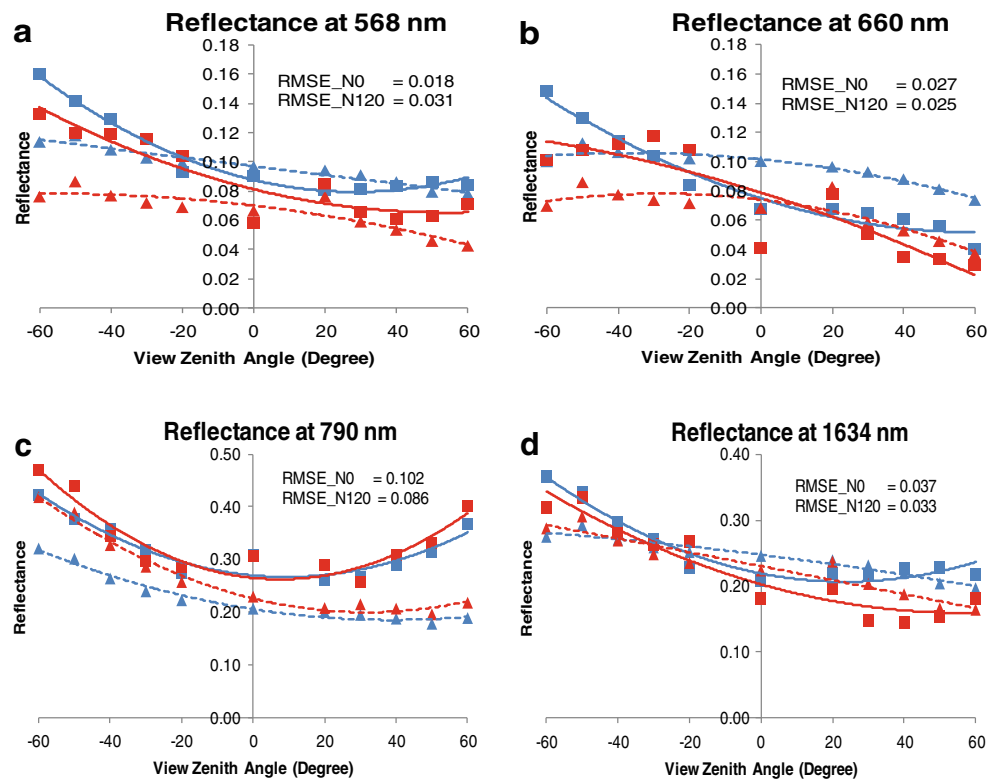
viewing results in higher reflectance. The highest reflectance at hotspot occurred because each leaf hide its own shadow when viewed from the direction of incident light (Hapke et al. 1996).

The hotspot reflectances at 568, 660 and 1,634 nm were significantly lower than at 790 nm. This may be due to significant absorption of radiation by leaf pigments or moisture. So, with the increase in the view zenith angle though the

Fig. 6 Comparison of the observed (square & line) and model simulated (triangle & dashed line) reflectance in the principal plane on 106 DAS for N_0 (blue) and N_{120} (red) at (**a**) 568 nm, (**b**) 660 nm, (**c**) 790 nm and (**d**) 1,634 nm
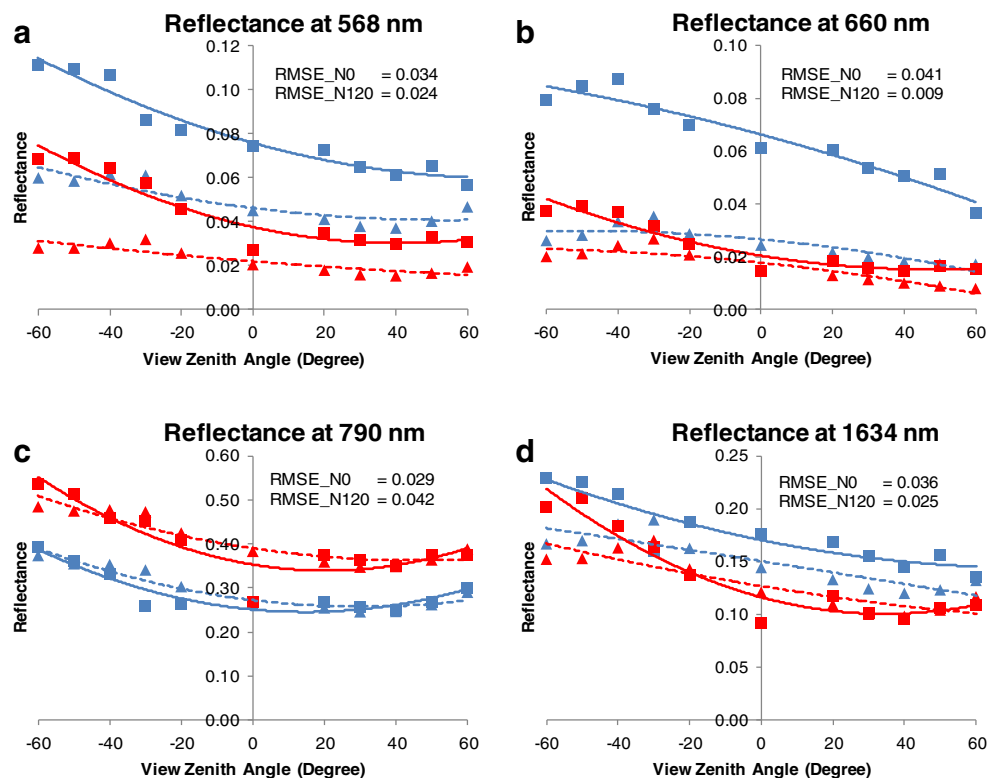
upper plant canopy area observed becomes more but proportionately the absorption also becomes more thus producing similar reflectance values. At the same time at these wavelengths, the minimum reflectance was observed in the forward scattering direction at higher view zenith angles. The cause of which can be attributed to the fact that in-spite of viewing higher proportion of upper plant canopy components with increasing view zenith angle, increased shadowing is also observed in the forward scattering direction (Hapke et al. 1996). Kimes (1984) suggested that the interaction of these two mechanisms result in the minimum reflectance at off-nadir angles in the forward scattering direction. So this factor produces the darkspot effect in the forward direction and hotspot in the backscattering direction where all shadows are hidden (Roman et al. 2011).

The occurrence of hotspot at 45° relative azimuth than in the principal plane in case of N_0 at 46 DAS may be due to sparse wheat canopy resulting in large exposure of soil background. The scattering by soil may be dominating as it is a stronger anisotropic reflector than vegetation (Kirchner et al. 1981). With the growth of canopy from 46 DAS to 106 DAS, broader hotspot was observed at all the four wavelengths. It may be the result of an increase in LAI, leaf size and planophilic leaf orientation and also due to the lowering of sun zenith angle with time (Qin and Goel 1995).

Unlike other wavelengths, the reflectance in the NIR was found to be more symmetric around nadir i.e. it increases in backward and forward scattering direction with the increment of the view zenith angles. This results in a shallow bowl shape reflectance spectra in principal plane as reported by (Walter-Shea et al. 1989) for alfalfa, Verbrugghe and Cierniewski (1995) for cotton, Sridhar et al. (2009) for wheat and Roman et al. (2011) for agricultural landscape. Shallow bowl shape in NIR band was very clearly seen in both the treatments and at two DAS in this study (Figs. 1 and 2). This can be explained by the scattering properties inherent in NIR reflectance. It increases with off-nadir angles due to viewing increasing multiple layering of leaves. It has been shown that additive reflectance occurs due to the transmittance and reflectance properties of the NIR (Swain and Davis 1978). The fifty per cent reflectance and transmittance properties typical of most leaves (Swain and Davis 1978), results in illumination of lower canopy layers that reflect back through the upper canopies thus increasing reflectance (Donovan et al. 1985). The extent of variation in BRF was more at 790 nm wavelength as compared to other wavelengths (Walter-Shea et al. 1989). It was also observed that on both the dates, the reflectance at 568, 660 and 1,634 was more in N_0 treatment, whereas at 790 nm it was more in N_{120}. It is because of the differential absorption and scattering at different wavelengths by leaf biophysical parameters like pigments, moisture content and structure. As N_0 was having lower chlorophyll and LAI, it resulted in higher reflectance in GREEN and RED bands and lower in NIR band. The reflectances in SWIR band in both N_0 and N_{120} were comparable on both the dates as moisture content was nearly same even though there were large differences in LAI. Jacquemoud et al. (2009) have also shown through a simulation study that LAI has no noticeable effect in the SWIR band where water absorption dominates.

Validation of PROSAIL Model

The spectral and directional sensitivity analysis of the PROSAIL model parameters has been documented in some studies (Bacour et al. 2002; Zarco-Tejada et al. 2003; Vohland and Jarmer, 2008; Jacquemoud et al. 2009). We observed that the canopy reflectance throughout the optical region was high in the backward direction where shadows were reduced. The PROSAIL model also showed similar increasing trend in the backward scattering direction as described in the sensitivity analysis by Jacquemoud et al. (2009). But the magnitude of increase was less than observed leading to underestimation by model at high view zenith angles. It points to the shortcoming in model to match the variations observed in the field across the view zenith angles in the principal plane, especially at high zenith angles. LAI clearly dominated both the forward and backward scattering direction in the NIR region resulting in a prominent bowl shape curve. The model showed better sensitivity in the NIR region and was able to simulate both the shape and the magnitude of the observed spectra except for the sparse canopy where background soil anisotropy dominated. This feature was also evident from significantly better simulation in NIR region during later part of crop growth i.e. (106 DAS) for both the treatments. The sensitivity of the model to simulate NIR reflectance at near nadir view was low due to higher exposure of the soil background. Hence, for retrieving LAI, nadir observations contain less information than at oblique angles. Besides, at the nadir position the model has largest influence of leaf orientation which is characterized by average leaf angle (*Angl*) (Jacquemoud et al. 2009).

The study results showed that model could simulate the hotspot position in all the wavelength regions at all growth stages in both the treatments. The view zenith angle at which model simulated hotspot corresponded to the solar zenith angle as at this position sensor views least shadow in the canopy. When compared with the observed hotspot position, it was found that they did not match exactly. The observed hotspot varied in a small range of view zenith around the simulated hotspot view zenith. It may be due to measurement errors caused by (a) assumption of constant sun geometry during 20–25 min of bi-directional reflectance measurement period, and (b) small asymmetry introduced in the goniometer due to uneven levelling in the field. The model, in general, underestimated reflectance at hotspot in all the wavelength bands and at the two growth stages. Andrieu et al. (1997) also showed for sugar beet that the model underestimated

reflectance for sun-sensor geometries close to the hotspot. This may be attributed to the approximation caused in the model by two-stream approach to compute multiple scattering in the canopy. Inclusion of four-stream isosector approximation may reduce this error which has much higher improvement for diffuse incident radiation than for direct incident radiation (Tian et al. 2007).

The model performance was poorer for sparse wheat canopy than for dense canopy. This was more pronounced in NIR region than at other wavelengths. In sparse canopies due to higher exposure of soil, the scattering properties of vegetation and soil combine to form a unique reflectance distribution (Donovan et al. 1985) which may not be captured in PROSAIL. Moreover in most of the variants of SAIL model, soil is assumed to be a Lambertian reflector (Jacquemoud et al. 2006, Verhoef and Bach 2007) though soil shows a strong anisotropic behaviour (Kirchner et al. 1981). SAIL showed high soil reflectance sensitivity in RED and NIR bands when corn canopy was low (Yao et al. 2008). Verhoef and Bach (2003) while using GeoSAIL, a variant of SAIL, also recommended that for a more realistic modelling of the BRF of sparse canopies, it will be necessary to incorporate the non-Lambertian reflection characteristics of bare soils into the GeoSAIL model. Inclusion of soil BRF anisotropy in the model is recommended for better simulation of sparse canopies.

The absolute errors in model simulations were very small in VIS region, followed by SWIR and highest were in NIR region. In terms of relative error (nRMSE), model showed lowest error in NIR region across dates and treatments while it was highest in VIS region. Andrieu et al. (1997) also observed that the relative difference between measured and simulated reflectances were lower in NIR than in the VIS region for sugar beet. Vohland and Jarmer (2008) have also reported that relative deviations between the simulated and the observed spectra were most striking in visible region leading to the poor estimation of Chlorophyll. Le Marie et al. (2004) have also pointed out the shortcomings of the PROSPECT model in the VIS domain. It is because in VIS region, absorption of radiation dominates while in NIR mostly scattering dominates. So, even small inconsistencies at shorter wavelengths become relatively large while opposite happens at longer wavelengths (Roman et al. 2011). It is also argued that there is always poor signal propagation from leaf to canopy scale resulting in poor estimation of leaf biochemical parameters from canopy reflectance (Jacquemoud et al. 1996). As the VIS band is having very low range of reflectance (2 to 9 % in our study) due to dominance of absorption, hence it is tough to model this region. This has implications in the retrieval of plant parameters especially leaf biochemical parameters such as chlorophyll whose information is coded in the VIS band. So, there is more chance of error in PROSAIL simulation of reflectance in VIS band, leading to poorer retrieval of leaf chlorophyll by model inversion.

The performance of the model was judged in the principal plane across all the view zenith angles because here surface reflectance anisotropy is more sensitive to canopy biophysical characteristics (Bacour et al. 2002). The observed reflectance showed bowl shape with view zenith angle at most wavelengths. The bowl shape was most prominent at 790 nm. The model simulated well the bowl shape reflectance pattern at 790 nm though there was considerable mismatch in the shape at other wavelengths. A close match was also obtained between the magnitude of observed and model simulated reflectance at 790 nm. As this wavelength region is sensitive to LAI and *Angl* (Jacquemoud et al. 2009), it indicates that model's assumptions of canopy as horizontally homogeneous, where leaves absorb, reflect, and transmit radiation (Verhoef 1984) hold good in case of wheat. Hence, any index which uses the NIR region to estimate the canopy property such as LAI will lead to a better retrieval of the same by model inversion.

The model showed underestimation in all the wavebands but its magnitude was much more in the backward scattering direction than in the forward scattering direction. The underestimation was higher in VIS band, especially at 568 nm wavelength and in backward scattering direction than in forward scattering direction. Bidirectional reflectance in the backward scattering direction is proportional to the leaf reflectance and in the forward scattering direction is proportional to the leaf transmittance (Verhoef 1984). As Le Marie (2004) has pointed out that the PROSPECT model has some problems in the visible domain due to a successive and indirect calibration of the original absorption coefficients. This may be the cause for the underestimation in the backscattering direction. Hence, improvements in the leaf absorption coefficients may improve the model performance. Similar to our observation, Verhoef and Bach (2007) have also reported that RMSE values were increasing with larger observation angles.

Conclusions

The study reconfirms the strong and consistent anisotropic patterns of reflectance in VIS, NIR and SWIR regions in response to change in the view zenith, sun zenith and relative azimuth at different growth stages of wheat. Though earlier studies have reported about anisotropy in VIS and NIR wavelengths, this study concluded that it is equally applicable in SWIR wavelength band. In case of sparse wheat canopy, the study found that hotspot at any wavelength may occur away from the principal plane due to the large exposure of soil background. Soil itself being strong anisotropic reflector modifies the crop anisotropic behaviour in a complex way to form a unique reflectance distribution. The hotspot becomes broader in wheat with the growth of crop due to increase in LAI, leaf size and planophilic orientation. These patterns are

of importance while using multi-angular satellite remote sensing for classification of crops and computing temporal profile of vegetation indices.

The performance evaluation of PROSAIL5B model using ground observations showed that the model very well simulated the shape of canopy spectra over optical wavelength region. A mismatch in the simulation of position of reflectance peak in GREEN wavelength region indicated deficiency in PROSPECT model which may be related to leaf absorption coefficient values assumed. The high underestimation in VIS band, especially in backscattering direction, bring forth the shortcoming of PROSPECT model and subsequent propagation of resulting errors through canopy layers in SAIL model. The model underestimated reflectance at hotspot in all wavelengths regions at different growth stages which may be mitigated by inclusion of four-stream isosector approximation instead of two-stream approach to compute multiple scattering in the canopy. The model performance was poor for sparse canopy and at nadir view due to large exposure of background soil which itself is highly anisotropic in nature. These results points out the limitation of assuming the soil as a Lambertian reflector in the model necessitating it to be modeled as a realistic non-Lambertian or anisotropic surface. Inclusion of canopy cover fraction into the model may further help to improve model performance under such conditions.

These results have implications for the retrieval of wheat biophysical parameters by PROSAIL inversion. The study indicated that the retrieval of leaf biochemical parameters, like, chlorophyll will be poorer due to large model error in VIS region (both at nadir and large view zenith angles) and also because absorption of radiation dominates in this region resulting in poor signal propagation from leaf to canopy scale. On the other hand retrieval of parameters like LAI, which have a dominating effect on NIR reflectance, will be better at any view zenith angle as model error is low in NIR region. Moreover in NIR region, the model is able to simulate well the typical shallow bowl shape reflectance pattern in the principal plane. As the modelled SWIR reflectance errors are in between that of VIS and NIR and are governed by leaf moisture, it is expected that the retrieval accuracy of leaf moisture may also be in between that of chlorophyll and LAI. But it may also be kept in mind that the dynamic range of leaf moisture is narrow for wheat which may result in its still poorer retrieval by model inversion. It is expected that the study shall help in understanding the associated uncertainties in inversion of PROSAIL model to retrieve crop biophysical parameters from multispectral images.

References

Andrieu, B., Baret, F., Jacquemoud, S., Malthus, T., & Stevent, M. (1997). Evaluation of an improved version of SAIL model for simulating bidirectional reflectance of sugarbeet canopies. *Remote Sensing of Environment, 60*, 247–257.

Bacour, C., Jacquemoud, S., Leroy, M., Hautecoeur, O., Weiss, M., Prevot, L., Bruguierd, N., Chaukid, H. (2002). Reliability of the estimation of vegetation characteristics by inversion of three canopy reflectance models on airborne polder data. *Agronomie: Agriculture and Environment, 22*, 555–565.

Barman, D., Sehgal, V. K., Sahoo, R. N., & Nagarajan, S. (2010). Relationship of bidirectional reflectance of wheat with biophysical parameters and its radiative transfer modeling using Prosail. *Journal of Indian Society of Remote Sensing, 38*, 35–44.

Darvishzadeh, R., Skidmore, A., Schlerf, M., & Atzberger, C. (2008). Inversion of a radiative transfer model for estimating vegetation LAI and chlorophyll in a heterogeneous grassland. *Remote Sensing of Environment, 112*(5), 2592–2604.

Donovan, S. Characterization and discrimination of selected vegetation canopies from field observations of bidirectional reflectances. M.Sc. Thesis, University of Maryland, USA, p 114, 1985.

Goel, N. S. (1989). Inversion of canopy reflectance models for estimation of biophysical parameters from reflectance data. In G. Asrar (Ed.), *Theory and Applications of Optical Remote Sensing* (pp. 205–251). New York: Wiley & Sons.

Hapke, B., DiMucci, D., Nelson, R., & Smythe, W. (1996). The cause of the hotspot in vegetation canopies and soils: shadow-hiding versus coherent backscatter. *Remote Sensing of Environment, 58*, 63–68.

Hiscox, J. D., & Israelstam, G. F. (1979). A method for the extraction of chlorophyll from leaf tissue without maceration. *Canadian Journal of Botany, 57*, 1332–1334.

Houborg, R., Soegaard, H., & Boegh, E. (2007). Combining vegetation index and model inversion methods for the extraction of key vegetation biophysical parameters using Terra and Aqua MODIS reflectance data. *Remote Sensing of Environment, 106*(1), 39–58.

Jacquemoud, S. (1993). Inversion of the PROSPECT + SAIL canopy reflectance model from AVIRIS equivalent spectra: theoretical study. *Remote Sensing of Environment, 44*(2–3), 281–292.

Jacquemoud, S., & Baret, F. (1990). PROSPECT: A model of leaf optical properties spectra. *Remote Sensing of Environment, 34*(2), 75–91.

Jacquemoud, S., Ustin, S. L., Verdebout, J., Schmuck, G., Andreoli, G., & Hosgood, B. (1996). Estimating leaf biochemistry using the PROSPECT leaf optical properties model. *Remote Sensing of Environment, 56*(194–202), 163–172.

Jacquemoud, S., Verhoef, W., Baret, F., Zarco-Tejada, P. J., Asner, G. P., Francois, C. & Ustin, S. L. PROSPECT SAIL: 15 Years of Use for Land Surface Characterization. Geoscience and Remote Sensing Symposium (IGARSS). IEEE international conference July 31, 2006- August 4, 2006.

Jacquemoud, S., Verhoef, W., Baret, F., Bacour, C., Zarco-Tejada, P. J., Asner, G. P., Francois, C., & Ustin, S. L. (2009). PROSPECT SAIL models: A review of use for vegetation characterization. *Remote Sensing of Environment, 113*, S56–S66.

Kimes, D. S., Holben, B. N., Tucker, C. J., & Newcomb, W. W. (1984). Optimal directional view angles for remote sensing missions. *International Journal of Remote Sensing, 5*(6), 887–908.

Kirchner, J. A., Schwetzler, C. C., & Smith, J. A. (1981). Simulated directional radiances of vegetation from satellite platforms. *International Journal of Remote Sensing, 2*(3), 253–264.

Le Maire, G., Francois, C., & Dufrene, E. (2004). Towards universal broad leaf chlorophyll indices using PROSPECT simulated database and hyperspectral reflectance measurements. *Remote Sensing of Environment, 89*, 1–28.

Meroni, M., Colombo, R., & Panigada, C. (2004). Inversion of a radiative transfer model with hyperspectral observations for LAI mapping in poplar plantations. *Remote Sensing of Environment, 92*(2), 195–206.

Qin, W., & Goel, N. S. (1995). An evaluation of hotspot models for vegetation canopies. *Remote Sensing Reviews, 13*, 121–159.

Roman, M. O., Gatebe, C. K., Schaaf, C. B., Poudyal, R., Wang, Z., & King, M. D. (2011). Variability in surface BRDF at different spatial scales (30 m–500 m) over a mixed agricultural landscape as retrieved from airborne and satellite spectral measurements. *Remote Sensing of Environment, 115*, 2184–2203.

Sridhar, V. N., Chaudhari, K. N., Tripathy, R., Chaurasia, S., Patel, N. K., Lunagaria, M., Guled, P. & Pandey, V. (2009). Multi-angular and temporal spectral signature study of wheat (*Triticum aestivum* L.) using a field goniometer, Scientific note SAC/RESA/AFEG/CMD/SN/06/2009, (p 42), Space Applications Centre, Ahmedabad,.

Swain, P. H., & Davis, S. M. (1978). *Remote Sensing: The Quantitative Approach*. New York: McGraw-Hill.

Tian, Y., Dickinson, R. E., & Zhou, L. (2007). Four-stream isosector approximation for canopy radiative transfer. *Journal of Geophysical Research, 112*(D4), 1–12.

Verbrugghe, M. & Cierniewski, J. (1995). Effects of sun and view geometries on cotton bidirectional reflectance. Test of a geometrical model. *Remote Sensing of Environment, 54*(3), 189–197.

Verhoef, W. (1984). Light scattering by leaf layers with application to canopy reflectance modelling: The SAIL model. *Remote Sensing of Environment, 16*(2), 125–141.

Verhoef, W., & Bach, H. (2003). Simulation of hyperspectral and directional radiance images using coupled biophysical and atmospheric radiative transfer models. *Remote Sensing of Environment, 87*, 23–41.

Verhoef, W., & Bach, H. (2007). Coupled soil–leaf-canopy and atmosphere radiative transfer modeling to simulate hyperspectral multi-angular surface reflectance and TOA radiance data. *Remote Sensing of Environment, 87*, 166–182.

Vohland, M., & Jarmer, T. (2008). Estimating structural and biochemical parameters for grassland from spectroradiometer data by radiative transfer modelling (PROSPECT SAIL). *International Journal of Remote Sensing, 29*(1), 191–209.

Welles, J. M., & Norman, J. M. (1991). Instrument for indirect measurement of canopy architecture. *Agronomy Journal, 83*(5), 818–825.

Yao, Y., Liu, Q., Liu, Q., & Li, X. (2008). LAI retrieval and uncertainty evaluations for typical row-planted crops at different growth stages. *Remote Sensing of Environment, 112*, 94–106.

Walter-Shea, E. A., Norman, J. M., & Blad, B. L. (1989). Leaf bidirectional reflectance and transmittance in corn and soybean. *Remote Sensing of Environment, 29*, 161–174.

Zarco-Tejada, P. J., Rueda, C. A., & Ustin, S. L. (2003). Water content estimation in vegetation with MODIS reflectance data and model inversion methods. *Remote Sensing of Environment, 85*(1), 109–124.